

ASSESSMENT OF WEAR EROSION IN PUMP IMPELLERS

by

Susanne Krüger

Core Technology and Tools Group

Sulzer Pumps Ltd.

Winterthur, Switzerland

Nicolas Martin

Project Engineer

Sulzer Markets and Technology Ltd.

Winterthur, Switzerland

and

Philippe Dupont

Head, Hydraulic Development Group

Sulzer Pumps Ltd.

Winterthur, Switzerland

Susanne Krüger is responsible for the Core Technology and Tools Group within the hydraulic development of the Sulzer Pump Division in Winterthur, Switzerland. She has worked in the turbomachinery business for six years and joined Sulzer in 2005.

Dr. Krüger holds an M.S. degree (Civil engineering) from the Technical University of Stuttgart, and a Ph.D. degree from Swiss Federal Institute of Technology of Zurich. After Post-Doc positions in fluid dynamics and biomechanics, she left university and entered industry.

Nicolas Martin is a Project Engineer within the Advanced Fluid Technology Group of Sulzer Markets and Technology, in Winterthur, Switzerland. He joined Sulzer in 2006.

Mr. Martin holds an M.S. degree (Mechanical Engineering) from the Swiss Federal Institute of Technology of Lausanne.



Philippe Dupont is Head of the Hydraulic Development Group of the Sulzer Pump Division in Winterthur, Switzerland. Before joining Sulzer in 1998, he headed the Cavitation Research Group of the Laboratory of Hydraulic Machines at the Swiss Federal Institute of Technology, in Lausanne, Switzerland.

Dr. Dupont received his M.S. degree (Mechanical Engineering, 1984) from the Swiss Federal Institute of Technology of Lausanne (EPFL) and his Ph.D. degree (1991) from the same technical school.

ABSTRACT

Wear erosion needs special attention in pump design as it can lead to severe damage of the pump and restrict its lifetime significantly. It therefore determines to a large extent the selection of a pump. During the design process it is essential to accurately predict possible erosion in pumps, adapt the design and select a proper material to minimize and prevent erosion.

Particle parameters like hardness, shape and size, material structure and hardness, as well as the flow pattern play an important role and determine erosion in pumps. Particle parameters are given

by the application and hence, can hardly be influenced, whereas the material of the pump is selectable. It is therefore crucial to carefully study the flow pattern in order to adapt the design to limit the occurrence of vortices and secondary flow structures to a minimum.

This paper describes the key parameters of erosion and presents two approaches for erosion prediction. The conventional approach is based on experimental data and empirical factors and estimates erosion in regions of the pump. Computational fluid dynamics enables the consideration of the entire flow pattern in a pump and therefore gives an overall and coherent picture.

This case study compares the erosion pattern of impellers resulting from experiments and simulation, investigates the influence of parameters like particle concentration, impingement angle, particle velocity, turbulent kinetic energy, and vortices secondary flow structures on the erosion pattern and correlates these parameters. It is clearly demonstrated that particle impingement angle and solids concentration play a dominant role in shock-like processes as they occur along the leading edge of an impeller blade. Contrarily, the flow pattern has a large impact on friction-like erosion processes, which occur along the blade, impeller trailing edge, tip clearance and side plate.

Both conventional empirical and modern numerical approaches allow only a qualitative prediction of the erosion pattern. The complex physical behavior with material hardening and softening as well as the resolution of the boundary layer show clear limitations for the quantitative prediction of friction-like erosion.

INTRODUCTION

Centrifugal pumps are often applied for the hydraulic transport of solids as it is the case in mining, production, extraction, or pulp and paper industry. In these cases, a large amount of solids is transported. Other cases are present, in which the solid appears in low concentration, as within the application of water and oil drawn from wells or rivers.

Both cases described above need special attention because the solid particles can yield hydro-abrasive wear (abrasion) of different pump components, which hence can lead to severe damage of the pump and restrict its life time significantly. Therefore, it determines to a large extent the selection of a pump. During the design process it is essential to accurately predict possible abrasion in pumps, adapt the design and select a proper material to minimize and prevent erosion. Therein, two aspects are relevant: the qualitative and the quantitative estimation.

Wear erosion is a complex subject with various relevant parameters. The erosion principles are discussed in the literature (Gülich, 2008; Prectl, 2001; Utz, 1986; Finnie, et al., 1992;

Finnie, 1995) based on experimental data. This paper summarizes the key parameters for particles, material and flow conditions.

The conventional approach used at Sulzer Pumps has been developed by Dr. Gülich (2008) and based on statistical data. Modern technologies available in commercial software packages based on computational fluid dynamics (CFD) offer methods to predict erosion in pumps. These methods are based on fluid flow calculations and either apply particle tracking methods or perform two-phase-computations to study the impact of solid particles on the pump. CFD can help to qualitatively predict and locate possible regions of erosion in a pump; however, they are not directly applicable for a quantitative estimation of the erosion rate. The main problem there is that erosion modifies the pump geometry with time and flow conditions change with it. This time-dependent process cannot be simulated with CFD.

This paper studies erosion of an open impeller at duty point. CFD computations are performed for the initial state (uneroded impeller geometry) and the final state (eroded impeller geometry). The impact of some key parameters on the impeller erosion distribution (initial and final state) is visualized and discussed.

EROSION PRINCIPLES

Different factors contribute to wear erosion. This section explains the two erosion processes that can be distinguished. Every contact between solid particle and pump component yields an interaction and contributes to wear. Hence, particle parameters and flow conditions need to be considered. This section further lists their key parameters.

Erosion Processes

The type of interaction between solid particle and pump component defines the erosion process. A particle sliding along a surface under pressure, with large tangential velocity component and a low impingement angle is a friction-like process. It mainly occurs along pressure or suction side of an impeller blade, at the tip clearance of an open impeller or along hub and shroud. Contrarily to that process, a particle hitting a pump component with a large normal velocity component and a high impingement angle is a shock-like process. This happens at the blade leading or trailing edge. Figure 1 illustrates these two processes with an eroded leading edge (shock-like process) and an eroded tip clearance (friction-like process).

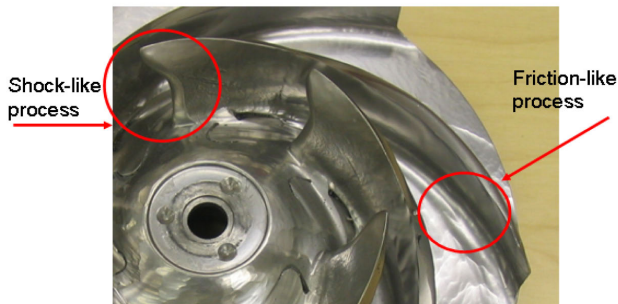


Figure 1. Wear in a Pump Impeller.

Key Parameters of Particles

Particle Concentration

The particle concentration has a strong influence on the erosion rate. The interaction of particles and pump component increases with the particle concentration, the ratio is roughly proportional. However, for high particle concentration the particles start interaction with each other, which yields in less contact with the component; the erosion rate then stays constant.

Impingement Angle

The erosion process strongly depends on the impingement angle α : for $\alpha=0$ degrees the process is friction-like, for $\alpha=90$ degrees the process is shock-like, and variations in between. Experiments showed that the maximum erosion rate is not only dependent on

the impingement angle but also on the material: for a brittle material it rises continuously to a maximum at $\alpha=90$ degrees, for a ductile metal it attains a maximum at about $\alpha=30$ degrees, and for elastomers at $\alpha=15$ degrees.

Particle Size

The kinetic energy of a particle impinging the wall at a given velocity and angle increases with the particle mass. In principle, the wear rate rises with the particle grain size, but not all tests exhibit this behavior. As a rule, the particle grain sizes comprise a spectrum that is characterized by the average particle diameter for which various definitions are in use. For example, the particle grain size is defined as the diameter at which either 50 percent of the solids mass are below/above this average diameter.

Particle Hardness and Shape

On one side, the erosion rate rises if the hardness of the solid particles exceeds the hardness of the material. On the other side, a sharp-angle particle generates more erosion than a sphere-like particle. Angular particles have a higher flow resistance coefficient than spherical, and, as a consequence, their flow paths are different.

Key Parameters for Flow Conditions

Flow Velocity

Theoretically, the erosion rises with a power of the kinetic energy and therefore with the flow velocity relative to the wall. Various experiments conducted show, however, a variation of this power coefficient between 0.9 and 5. Prechtl (2001) claims that for a power coefficient of 3, the erosion rate is stable. The material is softening with a power coefficient larger than 3 and hardening for a power coefficient smaller than 3.

Turbulence

Local excessive turbulence as induced by a roughened surface or geometrical irregularities can foster erosion. Turbulence induces a transport perpendicular to flow direction. If the mobility of the particles is large enough to overcome the reduced Reynolds number of the boundary layer, particles will be transported to the wall surfaces and cause erosion there.

Vortices and Secondary Flow

Vortices and secondary flow effects are caused by flow separation or deflection as they occur along sharp edges between vanes and side plates, in incident flow, at the tip clearances of open impellers, part load recirculation or rotating stall. Vortices and secondary flow effects strongly foster erosion and can lead to severe damage. Figure 2 illustrates vortices generated at the stagnation point at the blade leading edge yielding a flow separation along the blade pressure and suction side.

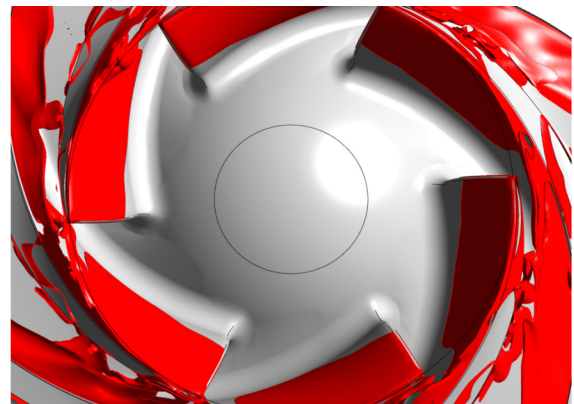


Figure 2. Vortices Generated at the Blade Leading Edge of an Open Impeller.

PREDICTION OF WEAR EROSION

From the erosion principles described above, flow conditions and particle—material—interaction are the key factors for wear erosion. The flow conditions are relevant for the motion of the particles in the fluid (particle accumulation and local concentration, direction of movement, velocities, impact angle, and turbulent kinetic energy). The type of interaction (shock-like or friction-like) and the material selection determine the magnitude of erosion.

With all these parameters contributing to wear erosion on a macro- and micro-structure level, it is obviously a very complex subject and the exact quantification of wear erosion—especially applicable for the design process—is impossible. Gülich (2008) has developed a rough empirical method for the quantitative prediction of wear erosion and also modern CFD codes offer possibilities. The following sections describe both methods.

Empirical Method

The empirical prediction of wear erosion follows the method given by Gülich (2008) and presented in Figure 3. The procedure is based on more than 100 test points available in open literature (Kießling, 1994).

Table 14.16 Estimation of metal loss due to hydro-abrasive wear			
Solids content c_s in kg/m^3	$\rho = \text{fluid density}$ $\rho_s = \text{solids density}$	$c_s = \frac{x}{1-x} \rho = \frac{c_v}{1-c_v} \rho_s$	$x = \frac{c_s}{\rho + c_s}$ (1)
Metal loss rate in mm/year Valid for: $c_s < 150 \text{ kg/m}^3$	$\frac{E_{R,a}}{E_{R,Ref}} = \frac{F_{Form} F_{Mat} F_{KG} F_{KF} F_{Fs}}{1 + c_s/\rho_s} \left(\frac{c_{s,eq}}{c_{s,Ref}} \right)^3 \left(\frac{w_{mix}}{w_{Ref}} \right)^3$ (2)		
	$E_{R,Ref} = 1 \text{ mm/year}; c_{s,Ref} = 1 \text{ kg/m}^3; w_{Ref} = 10 \text{ m/s}$		
Geometry		F_{Form}	Relevant velocity
Annular seals	Annular seals at impeller inlet, balance piston	3 to 5	$w = \sqrt{c_{ax}^2 + \left(\frac{u}{2}\right)^2}$ (3)
	Inter-stage seals	4 to 6	
Impeller sidewall gaps		3 to 5	$w \approx \frac{1}{2} u_2$ (4)
Impeller inlet	Leading edge	10 to 30	$w_1 = \sqrt{c_{1m}^2 + (u_1 - c_{1u})^2}$ (5)
	Corner vortex	10 to 20	
	Blade surface	6	
Impeller outlet	Blade pressure surface	10 to 20	$w_{2u} = u_2 - c_{2u}$ (6)
Diffuser inlet, volute cutwater	Leading edge, corner vortex	10 to 30	$c_{3u} = \frac{d_2 c_{2u}}{d_3}$ (7)
Cylindrical bore or channel [14.39]		3.3	$w = Q_{mix}/A$
Jet impinging at 90° on a structure [14.39]		68	Velocity at jet orifice
Rotating disk in wear device		0.03	$w = u_2$
Equivalent solids concentration $c_{s,eq}$	$c_{s,eq} = \sum \left(c_s \frac{H_s}{H_{Quartz}} \right)$	The fractions of a solids mixture are weighted according to their hardness. $H_{Quartz} = 1150 \text{ HV}$ (8)	
Grain size	$F_{KG} = \frac{d_s}{d_{Ref}}$	$d_{Ref} = 1 \text{ mm};$ for $d_s < 0.75 \cdot s$ ($s = \text{radial gap width}$)	(9)
Grain shape	$F_{KF} = 1$ for milled quartz sand; $F_{KF} = 0.6$ for round grains		
Grain hardness	$F_{Fs} = 1$ for quartz sand; $F_{Fs} = 0.017$ to 0.05 for lime stone		
Material hardness H_{Mat}	Ductile metals ($A > 5\%$)	$F_{Mat} = 1 + 1.3 \text{ Ln} \frac{H_{Ref}}{H_{Mat}}$ (10)	
	Stellite 20 $H_{Mat} = 670 \text{ HV}$ Ferro-Titanite $H_{Mat} = 535$ to 1150 HV	gap or bore jet	$F_{Mat} = 0.14 \frac{H_{Ref}}{H_{Mat}} - 0.063$ $F_{Mat} = 0.54 \frac{H_{Ref}}{H_{Mat}} - 0.22$ (11) (12)
$H_{Ref} = 700 \text{ HV}$	Material	$\frac{H_{Mat}}{\text{HV}}$	$\frac{F_{Mat}}{\text{Cylindrical bore}}$ $\frac{F_{Mat}}{\text{Orthogonal jet}}$
Conversion: $\text{HV} \approx 0.29 \cdot \text{R}_{cm}$ $\text{HV} \approx \text{HB}$	GX250CrMo15-3	876	0.25 0.6
	Hard metal 82.5 WC	1380	0.004 0.01 (estimated)
	Silicon carbide SiC	1500	0.0035 (estimated) 0.008
	Tungsten carbide WC		0.0012 0.003 (estimated)
	WC-CoCr spray coatings		0.006 to 0.04
Conversion of Rockwell to Vickers hardness	$\text{HV} = 125 \exp(0.029 \text{HR}_{c})$		

Figure 3. Empirical Prediction of Wear Erosion as Given by Gülich (2008).

The empirical model is based on the multiphase-flow approach and thus the mixture velocity w_{mix} is relevant for the wear rate (Equation (2)). Instead of considering the entire pump, the model splits up the pump into various regions (e.g., labyrinths, impeller side room, impeller inlet and outlet, diffuser). These regions are accounted for in empirical form factors F_{Form} , which strongly depend on the occurrence of vortices, recirculation and incident flow. These

secondary flow effects have to be taken into account carefully, as they can yield a variation of the form factors up to a multiplication of 3. The reaction of the material to abrasion depends on the hydro-abrasive wear and is expressed in material factors F_{Mat} , which were determined from measured data provided in (Vetter and Kießling, 1995). The tests were conducted with bores and orthogonal jets for different materials. Based on these tests, Equations (10) to (12) are relevant for the calculation of the material factor. Correspondingly, dimensionless factors for grain size F_{KG} (Equation (9)), grain form F_{KF} and solids hardness F_{HS} are applied.

A comparison among calculated and measured wear rates shows that Equation (2) can be of help for material selection. However, it must be emphasized that the above prediction yields an uncertainty that is large as many of the influencing factors are only a rough estimation.

Numerical Method

CFD programs offer different possibilities to account for wear erosion, which are all based on fluid flow computations. Then, they either apply particle tracking methods (Euler-Lagrange approach) or perform multiphase flow computations (Euler-Euler approach) to determine the impact of solid particles on the pump. Table 1 describes the advantages and disadvantages of both approaches.

Table 1. Discussion of Advantages and Disadvantages of Euler-Lagrange and Euler-Euler Approach.

	Euler – Lagrange approach	Euler – Euler approach
advantages	<ul style="list-style-type: none"> • Complete information on behavior of individual particles • Relatively cheap for a wide range of particle sizes • More flexible for a significant size distribution leading to different particle velocities 	<ul style="list-style-type: none"> • Complete information about particle phase (impacting conditions) • Applicable for a wide range of volume fraction • Turbulence is included
disadvantages	<ul style="list-style-type: none"> • Expensive if a large number of particles are tracked • Very expensive to include turbulence • Restricted to low particle volume fraction (the fraction of volume taken by the particles is not included in the continuous phase) • Particle rebounding parameters have to be specified • Particle impacting conditions are obtained with FORTRAN routines 	<ul style="list-style-type: none"> • Expensive if many sets of equations are used (different particle sizes) • Free-slip wall conditions are imposed at the walls • Computational effort

CASE STUDY

For the case study, a pump consisting of an axial inlet, a six-vane open impeller, a side plate, and a single volute is considered (refer to Figure 4). The erosion tests are performed with quartz sand having a density of 2610 kg/m^3 (534.5732 lb/ft^3) and a single particle size of $32 \mu\text{m}$ (0.00126 in). The fluid and solid phases are well mixed at the pump inlet and therefore assumed to be uniformly and homogeneously distributed with a volume fraction of 0.055.

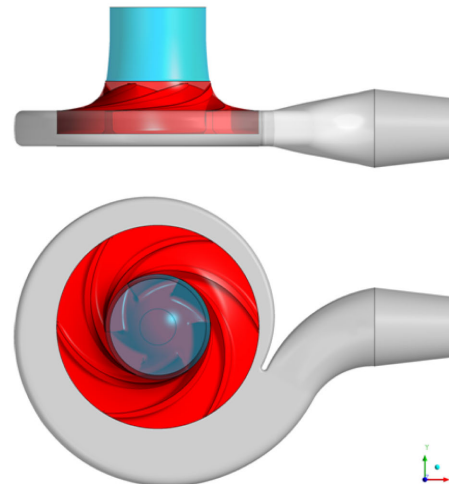


Figure 4. Pump Geometry Used in Case Study.

Despite the considerable computational effort, the Euler-Euler method was chosen because of its complete particle phase modeling and its direct access to particle impacting data. The CFD code used also offers different models to qualitatively and quantitatively account for erosion rate.

For the numerical simulations, average static pressure is imposed as outflow condition. At the walls, no-slip condition for the fluid phase and free-slip conditions for the particle phase are applied. The mesh consists of hexahedral elements and the mesh resolution is summarized in Table 2. The computations are run in unsteady mode using a transient rotor-stator interface to capture the unsteadiness of the flow.

Table 2. Mesh Resolution.

	Mesh Resolution			
	Suction channel	Impeller	Volute	Total
Number of Nodes	230'584	2'353'836	653'952	3'238'372

With the above described conditions, erosion tests were performed for three operating conditions: best efficiency point, part load and over load. However, in this study, we focus on best efficiency point. The eroded geometries were digitized with a 3D scan process to obtain the final state in electronic format and enable a comparison among new and worn states. The scan process delivers a cloud of points that are then connected by help of an algorithm to obtain the surfaces of the eroded impeller. As erosion is not uniform but varies from blade to blade, the comparison among original and final geometry is performed with a best fit. Figure 5 illustrates the original (lower left) and eroded (upper left) impeller and the best fit method at the trailing edge and in a circumferential section (right). Figure 6 visualizes the erosion depth of a single channel and blade. Obviously, strongest erosion occurs at the leading and trailing edge as well as blade pressure side tip clearance and along the hub. Minor erosion seems to be located along the blade and also at the hub. This could be an artifact due to differences in the geometry as the original impeller is derived from the theoretical model and not the manufactured impeller, which will differ from the theoretical one within the allowed tolerances.

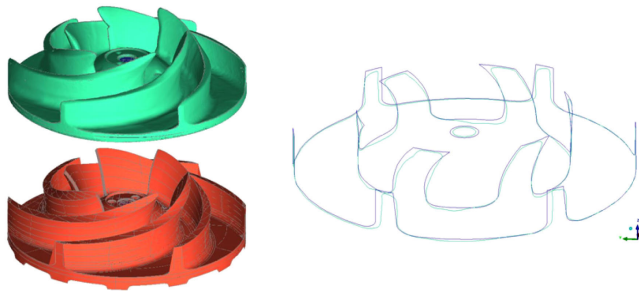


Figure 5. Comparison among Original (Red) and Eroded (Green) Impeller and Example for Best Fit (Right).

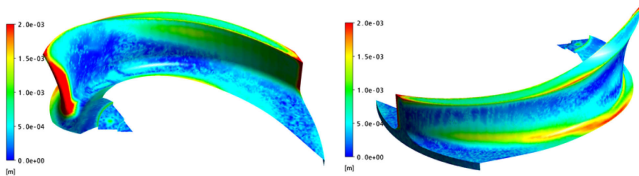


Figure 6. Eroded Depth of a Single Impeller Channel and Blade.

The key parameters for erosion are discussed within the section of erosion principles. CFD provides excellent tools to visualize the impact of single parameters. Within this study, the focus is brought on the key parameters particle impingement angle, solids concentration, and turbulent kinetic energy. Due to the significant changes in geometry before and after erosion, the key parameters and flow pattern are also expected to change.

Therefore, computations are performed on the initial and eroded geometry and key parameters are presented for these two (initial and eroded) states.

Figure 7 presents the structure in which the results are visualized and whether they are obtained through experiments (EXP) or computations (CFD). In analogy to this conventional approach (Equation (2)), an erosion factor is defined with:

$$Erosion\ factor = F_{KG} \cdot \left(\frac{C_{S,eq}}{C_{S,Ref}} \right) \cdot \left(\frac{W_{mix}}{W_{Ref}} \right)^3 \quad (13)$$

CFD	CFD	EXP
Particle Impingement Angle [degree]	Solids Concentration [-]	Measured Erosion Depth [m]
Erosion Factor [-]	Water Turbulence Kinetic Energy [-]	Location of the impeller (enlargement)

Figure 7. Structure of Result Visualization with Selected Key Parameters.

Contrary to Equation (2), in CFD there is no need to split up the geometry into different regions and take that into account with a form factor F_{Form} as the geometry is entirely reproduced.

Figure 8 shows the key parameters at the leading edge for the initial geometry (upper pictures) and the eroded geometry (final state, lower pictures). It is expected that erosion at the leading edge starts as a shock-like process rather close to tip clearance as a result of circulating particles. The high particle impingement angle along the entire leading edge (upper left picture) proves the expectation of a shock-like process. However, studying the solids concentration (upper central picture) indicates a particle accumulation in the upper center of the leading edge for the original state. Turbulence kinetic energy shows a peak at the leading edge close to tip clearance, which is most likely due to recirculation. This energy pushes the particles perpendicular to flow direction and therefore toward side plate and center of leading edge.

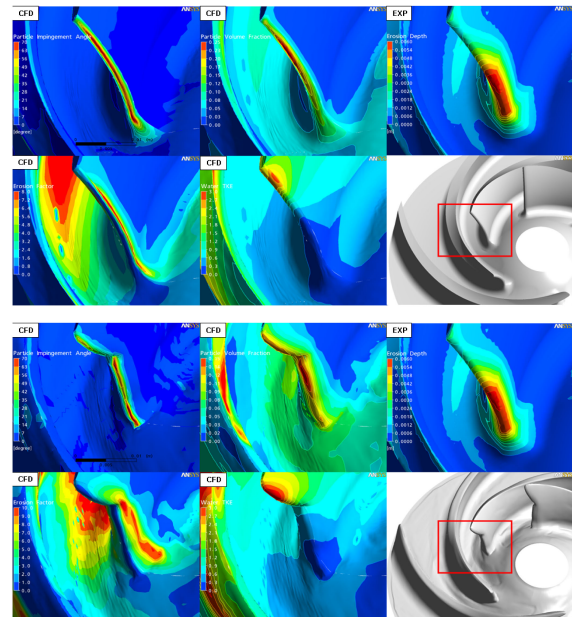


Figure 8. Key Erosion Parameters for Initial (Upper) and Eroded (Lower) Impeller, Focus on Leading Edge.

Looking at the final state of erosion (lower pictures), particle impingement angle and solids concentration reach peak values along the eroded region of the leading edge. Also, the erosion factor shows a qualitatively good agreement with the erosion depth.

Figure 9 illustrates erosion at trailing edge and Figure 10 along the blade. Both erosion processes are rather friction-like with a far smaller particle impingement angle but more driven by vortices and secondary flow structures like swirls. The particle accumulation is clearly visible in both Figure 9 and 10 when comparing the initial with the final state. Figure 11 presents the swirls in the impeller channel for initial state (left) and final state (right). The swirls are more pronounced not in strength but in amassment for the final state. They are responsible for the accumulation of particles along the transition hub/pressure side of blade and therefore the occurrence of erosion. At tip clearance, particle impingement angle, enhanced solids concentration and increasing turbulence kinetic energy all contribute together with the secondary flow structure to erosion there. The erosion factor shows no clear correlation with erosion depth both along blade and at trailing edge.

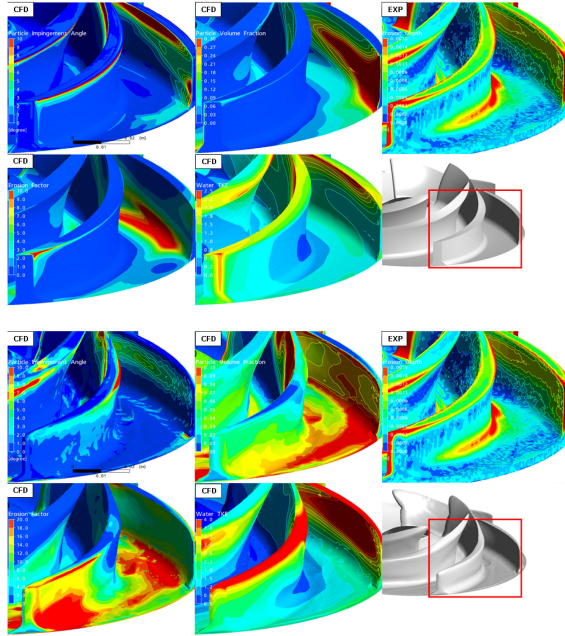


Figure 9. Key Erosion Parameters for Initial (Upper) and Eroded (Lower) Impeller, Focus on Trailing Edge.

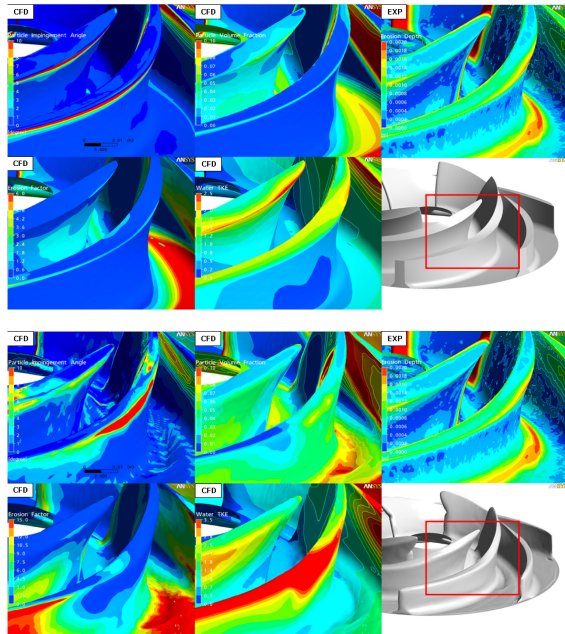


Figure 10. Key Erosion Parameters for Initial (Upper) and Eroded (Lower) Impeller, Focus on Blade.

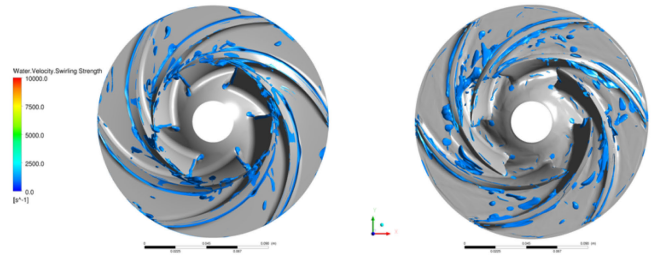


Figure 11. Swirls in the Impeller. Initial State (Left) and Final State (Right).

Figure 12 presents the key parameters and measured erosion at the side plate for initial and final state. Erosion at the side plate is dominated by a friction-like process; particle impingement plays a very minor role. Major erosion is expected to occur close to volute tongue as an effect of accumulated particles in that region. However, in the experiments distinct erosion occurs asymmetrically at the impeller eye. It is assumed that this is an effect of channel blockage due to the volute tongue. Particles accumulated at the impeller inlet surged through tip clearance with a high velocity would result in such erosion. This type of erosion cannot be reproduced by the current estimation approach (Equation (13)).

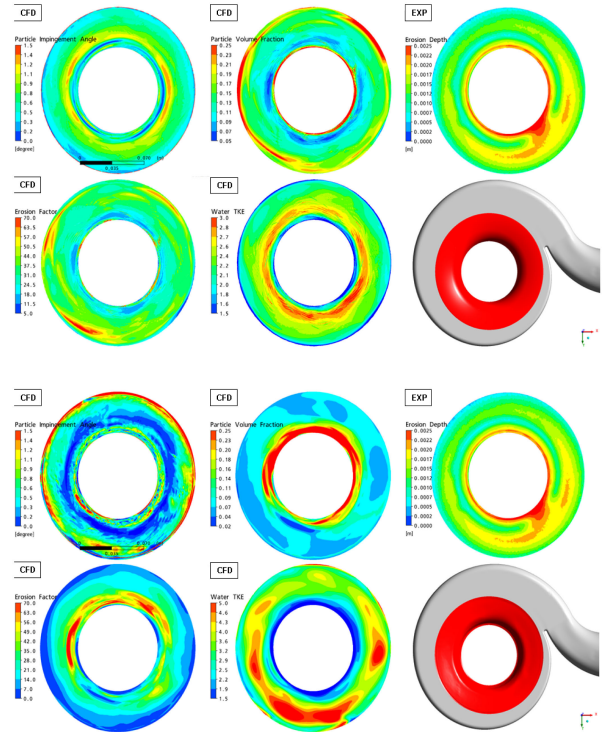


Figure 12. Key Erosion Parameters for Initial (Upper) and Eroded (Lower) Side Plate.

DISCUSSION AND CONCLUSION

Particle impingement angle, solids concentration and flow pattern represented by turbulence kinetic energy, vortices and secondary flow structures are key parameters for the occurrence of wear erosion. Two different methods for the wear estimation have been presented. Both approaches take into account particle and material parameters as well as flow velocity and solids concentration. The conventional method used at Sulzer Pumps is additionally based on form factors, which depend on the pump section. Nowadays, CFD techniques allow the simulation of erosion processes and allow a profound analysis of these key parameters.

The goal of this paper has been to study the influence of these key parameters with CFD and compare the results with experimental data. At the leading edge, erosion processes are shock-like and dominated by the particle impingement angle. High turbulence kinetic energy close to tip clearance pushes the particles to the center of the leading edge, being the main location of erosion. Initial and final state of erosion can both be simulated quite well.

Along the blade, trailing edge and side plate, erosion occurs in friction-like type. There, the flow pattern has a major impact. An inaccurate reproduction of vortices and secondary flow structures results in imprecise prediction of erosion. An additional deficiency is the numerical simulation of the interaction between wall boundary and particle as the particle is assumed to free-slip along the wall. Effects like material hardening or softening cannot be modeled.

Generally, the CFD can help to predict wear erosion on a qualitative level, e.g., foresee regions in which erosion is most likely to start. However, a quantitative prediction of erosion remains impossible at this time.

NOMENCLATURE

c_s	= Solids concentration (kg/m^3) or (lb/ft^3)
$c_{s,eq}$	= Equivalent solids concentration (kg/m^3) or (lb/ft^3)
$E_{r,a}$	= Metal loss rate (mm/year) or (in/year)
F_{Form}	= Form factor (-)
F_{Mat}	= Material factor (-)
F_{KG}	= Particle size factor (-)
F_{KF}	= Particle shape factor (-)
F_{Hs}	= Particle hardness factor (-)
w_{mix}	= Mixture velocity (m/s) or (ft/s)
w_{Ref}	= Reference value for velocity (10 m/s [$\sim 32.8 \text{ ft/s}$])

REFERENCES

- Finnie, I., 1995, "Some Reflections on the past and Future of Erosion," *Wear*, 186-187, pp. 1-10.
- Finnie, I., Stevick, G. R., and Ridgely, J. R., 1995, "The Influence of Impingement Angle on the Erosion of Ductile Metals by Angular Abrasive Particles," *Wear*, 152, pp. 91-98.
- Gülich, J., 2008, *Centrifugal Pumps*, Berlin Heidelberg: Springer-Verlag.
- Kießling, R., 1994, "Zur Modellierung und Simulation des hydroabrasiven Verschleißes ringförmiger Strömungsspalte," Ph.D. Thesis University of Erlangen-Nürnberg.
- Prechtel, W., 2001, "Verschleissverhalten mehrphasiger Werkstoffe unter hydroabrasiven Bedingungen," Ph.D. Thesis, University of Erlangen-Nürnberg.
- Utz, H., 1986, "Abrasion und Erosion—Grundlagen, Betriebliche Erfahrungen, Verminderung," Carl Hanser Verlag München Wien.
- Vetter, G. and Kießling, R., 1995, "Verschleißverhalten von Pumpenwerkstoffen bei hydroabrasiver Strahlbeanspruchung," *Konstruktion*, 47, pp. 186-190.